Study of excited D and D_s mesons in a relativized quark model*

Saba Noor† Faisal Akram Bilal Masud

Centre For High Energy Physics, University of the Punjab, Lahore (54590), Pakistan

Abstract: We use a modified relativistic quark model to study the properties of excited charmed and charmed strange mesons. We calculate the masses and wave functions of conventional charmed and charmed strange mesons incorporating both spin and S-D mixing effects and fit parameters of the potential model with known experimental states using differential evolution techniques. Using leading Born-Oppenheimer expansion, we compute the spectrum and wave functions of the first gluonic excited state of charmed and charmed strange mesons. We examine the effects of gluonic excitation on the spectrum of the resulting hybrid mesons. Using our calculated spectrum and wave functions, we determine the radiative transitions of the conventional and hybrid open charm mesons. We compare our calculations with experimental data and other works. We expect our results will be beneficial in the detection of charmed and charmed strange conventional and hybrid mesons.

Keywords: Charmed and Charmed Strange Mesons, Hybrid Charmed and Charmed Strange Mesons, Phenomenological potential model of mesons, Spectroscopy and Radiative transitions of Charmed and Charmed Strange mesons, Spectroscopy and Radiative transitions of Hybrid Charmed and Charmed Strange mesons

DOI: 10.1088/1674-1137/adec50 **CSTR:** 32044.14.ChinesePhysicsC.49113102

I. INTRODUCTION

Quantum Chromodynamics (QCD) is an experimentally well established theory of the strong interaction of quarks and gluons. However, describing the rich spectrum of hadrons from first principles is still challenging owing to the non-perturbative nature of QCD at low energy. Considering this difficulty, many models and theoretical approaches have been adopted to calculate hadron properties. The quark model, where applicable, is considered to be a convenient tool. According to the quark model, a conventional meson is a bound state of a quark and an antiquark. The model predicts that a meson can have only certain values of J^{PC}. The mesons with J^{PC} differing from quark-model values are called exotic mesons. In 1993, an exotic meson in the light quark sector having $J^{PC} = 1^{-+}$, was observed by the VES Collaboration [1]. Many exotic mesons have been observed since. Theoretically, exotic mesons could be glueball, tetra quark, or hybrid mesons. It is noted that the J^{PC} of these mesons can be allowed or forbidden by the quark model. Lattice QCD successfully describes these exotics [2–6]. Phenomenological models also provide a good description of the properties of exotic mesons [7–14]. In open flavor mesons where quarks and antiquarks have different flavors, C parity no longer remains a good quantum number. In this case, states are identified by their J^P values only. The states having the same J^P value are mixed. Indeed, all J^P states are mixed except 0^+ and 0^-. Mixing is either spin mixing or S-D mixing. This mixing will be discussed in detail in Section III. Incorporating mixing, where needed, we study the properties of hybrid as well as conventional mesons in the open charm meson sector, specifically charmed (D) mesons and charmed strange (D_s) mesons.

The gluonic field plays a dominant role in binding quarks. In conventional mesons, the gluonic field is in the ground state and in the excited state for hybrid mesons. We are particularly interested in studying the Π_u state, where the gluonic field is in its first excited state. We use the leading Born-Oppenheimer approximation (LBO) for calculating the spectrum of hybrid mesons. In this approximation, a hybrid meson is treated as a diatomic molecule in which quarks and gluons are considered as nuclei and electrons, respectively. There are two steps involved in applying LBO approximation. In the first step,

Received 10 February 2025; Accepted 4 July 2025; Published online 5 July 2025

* F. A. acknowledges HEC grant 20-15728/NRPU/R&D/HEC/2021, Pakistan

† E-mail: sabanoor87@gmail.com

the static potential energy of gluons is determined by treating quarks and antiquarks as spatially fixed, and in the second step, the motion of quarks is restored using this potential in the Schrödinger wave equation. The parity of the hybrid meson is $\varepsilon(-1)^{L+\Lambda+1}$, where Λ is the magnitude of the projection of total angular momentum of the gluonic field onto the molecular axis. For the Π_u potential, where the gluonic field is in its first excited state, $\Lambda=1$ and $\varepsilon=\pm1$ [2, 3].

The D and D_s meson domain has immense amounts of experimental data. The first two charmed mesons (D^0 and $D^\pm$) were discovered by the Mark I experiments in 1976 [15, 16]. Their J^P is 0^-. D^0 and $D^\pm$ have masses 1864.83 ± 0.05 MeV and 1869.58 ± 0.09 MeV, respectively. One year later, the first charmed strange meson ($D_s^\pm$) of $J^P=0^-$, was observed by the DASP Collaboration [17]. The mass of $D_s^\pm$ is 1968.34 ± 0.07 MeV [18]. In the same experiment, $D_s^{*\pm}$ meson was also discovered to have a mass of 2112.1 ± 0.4 MeV and $J^P=1^-$. At present, data for more than twenty well recognized states have been collected. Information of their masses, J^P values, and dozens of their decay modes are available in the Particle Data Group (PDG) listings [18]. In parallel, extensive work has been done to calculate their masses and other properties. Using Schrödinger-like wave equations in relativistic dynamics, the spectrum and wave functions of D and D_s mesons were calculated in Refs. [19−22]. In Ref. [20], strong and radiative transitions were reported. Refs. [23, 24] implemented the Dirac formalism to calculate the spectrum, radiative transitions, decay constant, and leptonic decay width of the D_s and D meson systems, respectively. In Ref. [25], the spectrum and wave functions of D and D_s mesons were obtained using the Bethe-Salpeter equation. Ref. [26] computed the spectrum of the heavy-light meson with the aid of a QCD motivated relativistic quark model. They investigated Regge trajectories as well. Using the Dirac Hamiltonian, Ref. [27] computed the mass spectra, wave functions, and hadronic transitions of heavy-light mesons. They also added leading order corrections in $1/m_{c,b}$. In Ref. [28], the spectrum of D and D_s mesons was calculated using Wilson twisted mass lattice QCD. Refs. [21, 22] discretized the relativistic wave equation using the Cornell potential (Coulomb plus linear potential). After calculating the masses and wavefunctions of mesons by diagonalizing the resulting Hamiltonian matrix, the spin dependent part of the Hamiltonian is added perturbatively because states with different principal quantum numbers can also have the same J^P. Thus, several principal quantum numbers collectively contribute to one mixed state (either spin mixed or S-D mixed). In Refs. [21, 22], the contribution of two to three principal quantum numbers was included to describe a mixed state. Another limitation of their work is that the perturbative effects of spin dependent potential are included in the masses but not in the wave function. This is understandable because first order perturbative correction to wave functions involves a sum over all possible internal states, which is extremely difficult to calculate. We adopted the same approach to solve the relativistic wave equation as in Refs. [21, 22], with improvements that address the limitations of the approach used in Refs. [21, 22]. Instead of including the spin dependent part of the Hamiltonian perturbatively, we also include spin dependent terms in the Hamiltonian matrix. For this purpose, we developed a system of coupled equations for mixed states. As we are solving the coupled equations nonperturbatively, we are not restricted to including the contribution of only two to three principal quantum numbers to describe a mixed state. Two charmed strange mesons named $D_{s0}^*(2317)^\pm$ and $D_{s1}(2460)^\pm$ attract special attention as the observed values of their masses are much lower than the quark model predictions. Attempts have been made to describe them through alternative models [29−32]. Extensive work has been carried out in the literature to determine the nature of these mesons. In some studies [33, 34], these states are interpreted as tetraquarks, while in others, $D_{s0}^*(2317)^\pm$ and $D_{s1}(2460)^\pm$ are regarded as DK and DK^* molecule states, respectively [35, 36]. In Refs. [37, 38], these states are well described by including coupled-channel effects. Ref. [37] suggests that these states are the mixtures of bare $c\bar{s}$ core and $D^{(*)}K$ component. In Refs. [20−22, 39], these states have been studied as conventional mesons. The exact structure of these particles is still an open question in hadron physics.

In this study, we calculate masses, wave functions, and radiative transitions of conventional as well as hybrid D and D_s mesons, incorporating spin and S-D mixing effects on spectrum and wave functions. Unlike previous studies, we solve the Schrödinger-type equation using the full semi-relativistic Hamiltonian, including the spin-dependent part. This approach allows us to study both spin effects and S-D mixing without relying on perturbation theory.

This paper is structured as follows: In Section II, we describe our potential model for conventional and hybrid mesons. We use an extended version of the famous GI model. For the hybrid mesons, we add the potential model of gluonic excitation, which we have suggested in a previous study. In this study, we improve the parameter fitting of our proposed gluonic excited potential model by considering the latest lattice data [6]. In Section III, the phenomena of state mixing are examined. We distinguish two categories of mixed states. We also discuss the effects of the spin dependent part of the potential model on the spectrum. In Section IV, we describe our relativistic wave equation. We explicitly describe how we calculate masses and wave functions of mesons using a relativistic wave equation. State mixing effects in the Hamiltonian matrix are discussed as well. Radiative transitions of charmed and charmed strange mesons are reviewed in Section V. In the last section, we report our results and concluding remarks based on our calculations.

II. EFFECTIVE POTENTIAL MODEL OF MESONS

Phenomenological potential models are successful in describing various properties of heavy quark mesons, particularly mass [19–25, 40–43]. Among the suggested models, the GI model [19] is the most well-known. In this study, we have used it with some modifications.

A. Potential model of conventional mesons

The conventional D and D_s mesons are bound states of heavy quarks ($Q = c$) and a light antiquarks ($\bar{q} = \bar{u}/\bar{d}$, $\bar{s}$), respectively. The potential model of a conventional meson $V_{Q\bar{q}}(r)$ is

$$V_{Q\bar{q}}(r) = -\frac{4\alpha_s(r)}{3r} + br + c + V_{\text{spin-dep}}(r), \tag{1}$$

where r is the inter-quark distance. The first term of the potential model, called the Coulomb term, is calculated by one gluon exchange diagram in perturbation theory. It determines the behavior of potentials at small distances. $\alpha_s(r)$ is a strong running coupling constant of QCD. Its parameterization is given by [19]

$$\alpha_s(r) = \sum_{k=1}^{3} \alpha_k \frac{2}{\sqrt{\pi}} \int_0^{\gamma_k r} \mathrm{e}^{-x^2} \mathrm{d}x, \tag{2}$$

where α_k's and γ_k's are free parameters. In this study, we take $\gamma_1 = \frac{1}{2}$, $\gamma_2 = \frac{\sqrt{10}}{2}$, and $\gamma_3 = \frac{\sqrt{1000}}{2}$, as in Ref. [19]. With this choice of γ's, α_2 and α_3 control the shape of running coupling at small distances (large Q^2), where it is already fixed by pQCD. This allows us to fix $\alpha_2 = 0.16$ and $\alpha_3 = 0.20$ through fitting with 2-loop running coupling. Consequently, the parameter α_1 (or $\alpha_s^c \equiv \alpha_1 + \alpha_2 + \alpha_3$), which controls the shape of the running coupling in the infrared region, is treated as a free parameter that is fixed via spectroscopy [19, 44]. Figure 1 shows the comparisons of $\alpha_s(Q^2)$ of the parametrized model with the results obtained using our fitted $\alpha_s^c = 0.24$ and pQCD 2-loop result.

The second term of the potential is the confinement term, which dominates at large distances. The parameter b represents the string tension and is determined by fitting the spectrum. The third term, c, is also treated as a free parameter in the potential model. The last part of the potential model, the spin dependent term $V_{\text{spin-dep}}(r)$, is defined as follows:

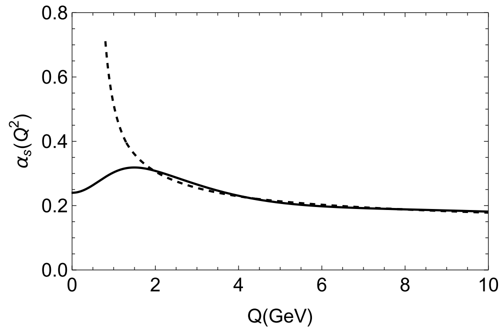

Fig. 1. Strong running coupling constant in the momentum space. The solid curve represents data from the parametrized model and the dotted curve represents data from QCD perturbative calculations up to two loop corrections.

$$V_{\text{spin-dep}}(r) = V_{\text{hyp}}(r) + V_T(r) + V_{\text{so}}(r), \tag{3}$$

where $V_{\text{hyp}}(r)$ is the spin-spin contact hyperfine interaction [43]. It is defined as

$$V_{\text{hyp}}(r) = \frac{32\pi}{9m_Q\tilde{m}_{q1}}\alpha_s(r)\left(\frac{\sigma}{\sqrt{\pi}}\right)^3 \mathrm{e}^{-\sigma^2 r^2}\mathbf{S_Q}\cdot\mathbf{S_{\bar{q}}}, \tag{4}$$

where $\langle \mathbf{S_Q}\cdot\mathbf{S_{\bar{q}}}\rangle = \frac{S(S+1)}{2} - \frac{3}{4}$. In Ref. [19], the parameter σ is

$$\sigma = \sqrt{\sigma_0^2\left(\frac{1}{2}+\frac{1}{2}\left(\frac{4m_Q m_{\bar{q}}}{(m_Q+m_{\bar{q}})^2}\right)^4\right) + s_0^2\left(\frac{2m_Q m_{\bar{q}}}{m_Q+m_{\bar{q}}}\right)^2}.$$

Numerical values of parameters σ_0 and s_0 are determined by fitting the spectrum. In Eq. (3), $V_T(r)$ is the tensor term defined as

$$V_T(r) = \frac{4\alpha_s(r)}{m_Q\tilde{m}_{q2}}\frac{T}{r^3}, \tag{5}$$

where T is the tensor operator:

$$T = \mathbf{S_Q}\cdot\hat{r}\mathbf{S_{\bar{q}}}\cdot\hat{r} - \frac{1}{3}\mathbf{S_Q}\cdot\mathbf{S_{\bar{q}}}. \tag{6}$$

The tensor operator has nonvanishing matrix elements only between $L > 0$ and spin triplet states. The diagonal Hamiltonian matrix entries of the tensor operator are [43]

$$\langle {}^3L_J|T|{}^3L_J\rangle = \begin{cases} -\dfrac{L}{6(2L+3)} & J = L+1 \\ \dfrac{1}{6} & J = L \\ -\dfrac{(L+1)}{6(2L-1)} & J = L-1. \end{cases} \tag{7}$$

To study S-D mixed states, we require the off diagonal matrix element of the tensor operator

$$\langle ^3L_J|T|^3L'_J\rangle = \frac{\sqrt{(L+1)(L+2)}}{2(2L+3)}, \tag{8}$$

where $L^{'} = L+2$. In Eq. (3), $V_{\rm so}(r)$ is the spin-orbit interaction term. It consists of two parts, such that

$$V_{\rm so}(r) = V_{\rm sov}(r) + V_{\rm sos}(r). \tag{9}$$

Here, $V_{\rm sov}(r)$ is a spin-orbit vector:

$$V_{\rm sov}(r) = \frac{4}{3}\frac{\alpha_s(r)}{r^3}\left[\left(\frac{1}{2m_Q^2}+\frac{1}{m_Q\tilde{m}_{q3}}\right)\mathbf{L}\cdot\mathbf{S_Q} + \left(\frac{1}{2\tilde{m}_{q3}^2}+\frac{1}{m_Q\tilde{m}_{q3}}\right)\mathbf{L}\cdot\mathbf{S_{\bar{q}}}\right], \tag{10}$$

and $V_{\rm sos}(r)$ is the spin-orbit scalar part of the spin-orbit interaction term

$$V_{\rm sos}(r) = -\frac{b}{r}\left(\frac{\mathbf{L}\cdot\mathbf{S_Q}}{2m_Q^2}+\frac{\mathbf{L}\cdot\mathbf{S_{\bar{q}}}}{2\tilde{m}_{q4}^2}\right). \tag{11}$$

For diagonal Hamiltonian matrices, $\langle\mathbf{L}\cdot\mathbf{S_Q}\rangle = \langle\mathbf{L}\cdot\mathbf{S_{\bar{q}}}\rangle = \dfrac{\langle\mathbf{L}\cdot\mathbf{S}\rangle}{2}$, where $\langle\mathbf{L}\cdot\mathbf{S}\rangle$ is

$$\langle ^1L_L|\mathbf{L}\cdot\mathbf{S}|^1L_L\rangle = \langle ^3L_L|\mathbf{L}\cdot\mathbf{S}|^3L_L\rangle = \frac{J(J+1)-L(L+1)-S(S+1)}{2}. \tag{12}$$

To study spin mixed states, we require the following matrix element of the $\langle\mathbf{L.S_Q}\rangle$ and $\langle\mathbf{L.S_{\bar{q}}}\rangle$ operators:

$$\langle ^1L_L|\mathbf{L}\cdot\mathbf{S_Q}|^3L_L\rangle = -\frac{\sqrt{L(L+1)}}{2}, \tag{13}$$

$$\langle ^1L_L|\mathbf{L}\cdot\mathbf{S_{\bar{q}}}|^3L_L\rangle = \frac{\sqrt{L(L+1)}}{2}. \tag{14}$$

The form of the spin dependent part of the potential model is extracted from leading order perturbation theory in the non-relativistic approximation. However, this is not a good approximation, particularly for light quarks in heavy light mesons. Owing to the presence of a light quark in charmed and charmed strange mesons, it is essential to incorporate relativistic effects. These effects modify the potential in two distinct ways [19]: First, the quark antiquark separation (r) becomes smeared over a distance on the order of the inverse quark mass. By introducing the smearing function [19], smearing over $1/r^3$ terms in the spin dependent part of the potential model is incorporated. Smearing also eliminates instability in the solution of the relativistic wave equation, which occurs at short distances due to the $1/r^3$ term in the spin dependent potential model and makes the solution stable even at short distances. The second way to incorporate relativistic effects is to make the potential model momentum dependent. Momentum dependence in the spin dependent term can be effectively incorporated by introducing multiple constant factors. This modification is applied only to the light quark, as the momentum terms for the heavy quark effectively drop out. As momentum dependence modifies each spin interaction term differently, we introduce multiple constants (ϵ_i), each specific to a particular interaction. Here, i = 1, 2, 3, and 4 correspond to the hyperfine term, tensor term, spin orbit vector term, and spin orbit scalar term, respectively. These constants are absorbed into the light quark mass, allowing us to define an interaction dependent effective mass as [21, 22] $\tilde{m}_{qi} = \tilde{m}_q\epsilon_i$. The numerical values of these parameters are obtained by fitting the spectrum. It is noteworthy that because we are treating m_q as a free parameter, we must take $\epsilon_1 = 1$.

B. Potential model of hybrid mesons

In hybrid mesons, the gluonic field is in an excited state. In this case, the quark antiquark potential can be written as

$$V_{\rm hybrid}(r) = V_{Q\bar{q}}(r) + V_g(r), \tag{15}$$

where $V_{Q\bar{q}}(r)$ is the potential for conventional mesons appearing in Eq. (1). $V_g(r)$ is the potential energy difference between the ground and first excited state of the gluonic field. The proposed model of $V_g(r)$ is [45]

$$V_g(r) = A{\rm e}^{-Br^{\nu}} + \frac{\mu}{r}. \tag{16}$$

Numerical values of parameters A, B, ν, and μ are determined by fitting the model with recent lattice data taken from Fig. 2 of Ref. [6]. The parameters are estim-

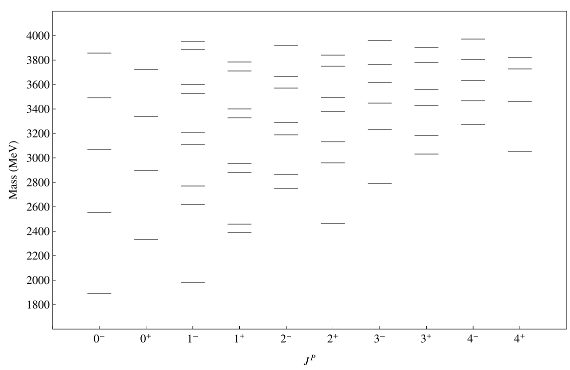

Fig. 2. Conventional charmed meson spectrum.

ated by minimizing the χ^2 function using a global numerical optimization algorithm. Our improved fitted values of A, B, ν, and μ are 3.0552 GeV, 0.9369 GeV, 0.3881, and -0.0025, respectively. There is no underlying physical motivation for using the above model to fit the gluon potential, other than the fact that it provides a good fit to the lattice data.

III. MIXED STATES

In the D and D_s mesons, charge conjugation is not a conserved quantum number, and states are described only by their J^P values. States having the same value of J^P can mix. Except for 0^- and 0^+, all possible values of J^P have mixed states. State mixing is categorized into two types: *S-D* mixing and spin mixing.

A. *S-D* mixing

In the mixing of spin triplet states ($^3L_J \leftrightarrow {}^3L'_J$), orbital angular momentum is changed ($L' = L+2$), whereas total angular momentum remains same ($J = L+1 = L'-1$). The $^3S_1$ and $^3D_1$ states have the same values of J^P. Therefore, they are mixed. Similarly, $^3P_2 \leftrightarrow {}^3F_2$, $^3D_3 \leftrightarrow {}^3G_3$, $^3F_4 \leftrightarrow {}^3H_4$, $^3G_5 \leftrightarrow {}^3I_5$ etc., are all referred to as *S-D* mixed states. *S-D* mixing occurs due to the tensor operator in the potential model, as this operator does not conserve orbital angular momentum.

B. Spin mixing

The spin-orbit interaction term in the potential model does not conserve the total spin of quarks and antiquarks. It causes mixing between the spin triplet and spin singlet states ($^1L_L \leftrightarrow {}^3L_L$), for which $J = L$. In this case, possible combinations of mixed states are $^1P_1 \leftrightarrow {}^3P_1$, $^1D_2 \leftrightarrow {}^3D_2$, $^1F_3 \leftrightarrow {}^3F_3$, $^1G_4 \leftrightarrow {}^3G_4$, $^1H_5 \leftrightarrow {}^3H_5$ etc.

IV. RELATIVISTIC WAVE EQUATION

In the study of charmed and charmed strange mesons, relativistic effects must be incorporated due to the presence of a light quark. To account for this, we use a relativistic wave equation to investigate the bound states of charmed and charmed strange mesons [19]. The Schrödinger-type equation in relativistic dynamics is

$$H\psi(\mathbf{r}) = E\psi(\mathbf{r}), \tag{17}$$

where $\psi(\mathbf{r})$ and E are the wave function and energy of mesons, respectively. H is an effective Hamiltonian of mesons:

$$H = \sqrt{\mathbf{p}^2 + m_Q^2} + \sqrt{\mathbf{p}^2 + m_{\bar{q}}^2} + V(\mathbf{r}), \tag{18}$$

where $\mathbf{p}$ is the center-of-mass momentum of quarks such that $\mathbf{p} = \mathbf{p}_Q = -\mathbf{p}_{\bar{q}}$. $\mathbf{p}_Q$ and $\mathbf{p}_{\bar{q}}$ are momenta of quarks and antiquarks. m_Q and $m_{\bar{q}}$ are masses of heavy quarks (*i.e.*, charm quark) and light antiquarks, respectively. $V(\mathbf{r})$ is the effective potential of the bound state of the quark and antiquark system, as discussed in Section II. We assumed a central potential, *i.e.*, $V(\mathbf{r}) \equiv V(r)$ as our potential. For conventional mesons, $V(r) = V_{Q\bar{q}}(r)$ (appearing in Eq. (1)) and for hybrid mesons, $V(r) = V_{\text{hybrid}}(r)$ (appearing in Eq. (15)).

A conventional meson is a bound state of a quark and an antiquark. When the distance between them becomes sufficiently large, the wavefunction vanishes. We denote the distance at which the wavefunction vanishes as R. To solve Eq. (17), we construct a matrix representation of the relativistic Hamiltonian H using spherical Bessel functions as the basis. Diagonalizing the resulting Hamiltonian matrix yields $\psi(\mathbf{r})$ and E. For the unmixed state (*i.e.*, 0^-, 0^+), the radial wave function is

$$R_l(r) = \sum_{i=1}^{N} c_i \frac{a_i}{R} j_l\left(\frac{a_i r}{R}\right), \tag{19}$$

where $c_i s$ are expansion coefficients, j_l is the spherical Bessel function, and a_i is the i^{th} root of the spherical Bessel function, such that $j_l(a_i) = 0$. In this basis, Eq. (17) reduces to that of Ref. [22]

$$\frac{2\Delta a_i a_i^2}{\pi R^3} N_{li}^2 \left(\sqrt{\left(\frac{a_i}{R}\right)^2 + m_Q^2} + \sqrt{\left(\frac{a_i}{R}\right)^2 + m_{\bar{q}}^2} \right) c_i + \sum_{j=1}^{N} \frac{a_j}{N_{li}^2 a_i} \int_0^R \mathrm{d}r V(r) r^2 j_l\left(\frac{a_i r}{R}\right) j_l\left(\frac{a_j r}{R}\right) c_j = E c_i, \tag{20}$$

where N_{li}^2 is the radial integral of the spherical Bessel function given by

$$N_{li}^2 = \int_0^R \mathrm{d}r' r'^2 j_l\left(\frac{a_i r'}{R}\right)^2. \tag{21}$$

In Eq. (20), the Hamiltonian matrix is of the order $N\times N$. By diagonalizing this matrix, we obtain N eigenvalues and corresponding eigenfunctions. Each eigenvalue and eigenfunction is associated with a specific value of the radial quantum number. For each eigenvector, the corresponding radial wavefunction is constructed using Eq. (19). For mixed states, $\psi(\mathbf{r})$ is a combination of two states. For spin mixed states, $\psi(\mathbf{r})$ is

$$\psi(\mathbf{r}) = \sum_{i=1}^{N} c_i^{(1)} \frac{a_i}{R} j_l\left(\frac{a_i r}{R}\right) |^1L_L\rangle_{\hat{r}} + \sum_{i=1}^{N} c_i^{(2)} \frac{a_i}{R} j_l\left(\frac{a_i r}{R}\right) |^3L_L\rangle_{\hat{r}}, \tag{22}$$

where a_i is the zeroth roots of the spherical Bessel function corresponding to the L orbital angular momentum. $c_i^{(1)}$ and $c_i^{(2)}$ are the expansion coefficients associated to the $|^1L_L\rangle_{\hat{r}}$ and $|^3L_L\rangle_{\hat{r}}$ states, respectively, which are defined as

$$|^1L_L\rangle_{\hat{r}} = |0,0\rangle_s Y_{L,L}(\hat{r}), \tag{23}$$

$$|^3L_L\rangle_{\hat{r}} = \sum_{m_s} C_{m_s}|1,m_s\rangle_s Y_{L,L-m_s}(\hat{r}). \tag{24}$$

where C_{m_s} is the Clebsch-Gorden coefficient. In mixed states, Eq. (17) is reduced to two coupled equations. For spin mixed states, the equations are

$$\frac{2}{\pi R^3}\Delta a_i a_i^2 N_{li}^2\left(\sqrt{\left(\frac{a_i}{R}\right)^2+m_Q^2}+\sqrt{\left(\frac{a_i}{R}\right)^2+m_{\bar{q}}^2}\right)c_i^{(1)} + \sum_{j=1}^{N}\frac{a_j}{N_{li}^2 a_i}\int_0^R \mathrm{d}r\left(\langle V\rangle_{11}c_j^{(1)}+\langle V\rangle_{12}c_j^{(2)}\right) r^2 j_l\left(\frac{a_i r}{R}\right)j_l\left(\frac{a_j r}{R}\right)=Ec_i^{(1)}, \tag{25}$$

$$\frac{2}{\pi R^3}\Delta a_i a_i^2 N_{li}^2\left(\sqrt{\left(\frac{a_i}{R}\right)^2+m_Q^2}+\sqrt{\left(\frac{a_i}{R}\right)^2+m_{\bar{q}}^2}\right)c_i^{(2)} + \sum_{j=1}^{N}\frac{a_j}{N_{li}^2 a_i}\int_0^R \mathrm{d}r\left(\langle V\rangle_{21}c_j^{(1)}+\langle V\rangle_{22}c_j^{(2)}\right) r^2 j_l\left(\frac{a_i r}{R}\right)j_l\left(\frac{a_j r}{R}\right)=Ec_i^{(2)}. \tag{26}$$

The Hamiltonian matrix H can be expressed through four $N\times N$ matrices H_{11}, H_{12}, H_{21}, and H_{22} as follows:

$$H=\begin{pmatrix} H_{11} & H_{12}\\ H_{21} & H_{22}\end{pmatrix}. \tag{27}$$

H_{11} and H_{12} are read off from Eq. (25), and H_{21} and H_{22} from Eq. (26). The kinetic energy of mesons contributes only to diagonal Hamiltonian matrices (H_{11}, H_{22}). $\langle V\rangle_{11}$, $\langle V\rangle_{12}$, $\langle V\rangle_{21}$, and $\langle V\rangle_{22}$ are the potential energy matrix elements of H_{11}, H_{12}, H_{21}, and H_{22}, respectively. The definition of the potential energy matrix elements is mentioned in Table 1. Notably, the mixing of the states occurs due to off-diagonal Hamiltonian matrices (H_{12}, H_{21}). For the mixed spin state, contributions to $\langle V\rangle_{12}$ and $\langle V\rangle_{21}$ are from spin-orbit terms of the potential energy.

In the S-D mixed states, $\psi(\mathbf{r})$ is

Table 1. Definition of the potential energy matrix elements for the spin and S-D mixed states.

Potential energy matrix elements	Spin mixed state	S-D mixed state
$\langle V\rangle_{11}$	$\langle ^1L_L\|V\|^1L_L\rangle$	$\langle ^3L_J\|V\|^3L_J\rangle$
$\langle V\rangle_{12}$	$\langle ^1L_L\|V_{so}\|^3L_L\rangle$	$\langle ^3L_J\|V_T\|^3L'_J\rangle$
$\langle V\rangle_{21}$	$\langle ^3L_L\|V_{so}\|^1L_L\rangle$	$\langle ^3L'_J\|V_T\|^3L_J\rangle$
$\langle V\rangle_{22}$	$\langle ^3L_L\|V\|^3L_L\rangle$	$\langle ^3L'_J\|V\|^3L'_J\rangle$

$$\psi(\mathbf{r})=\sum_{i=1}^{N}c_i^{(1)}\frac{a_i}{R}j_l\left(\frac{a_i r}{R}\right)|^3L_J\rangle_{\hat{r}}+\sum_{i=1}^{N}c_i^{(2)}\frac{a'_i}{R}j_{l'}\left(\frac{a'_i r}{R}\right)|^3L'_J\rangle_{\hat{r}}, \tag{28}$$

where a_i and a'_i are the zeroth roots of the spherical Bessel function corresponding to L and L' orbital angular momenta, respectively. In the S-D mixed states, $c_i^{(1)}$ and $c_i^{(2)}$ are expansion coefficients associated to the $|^3L_J\rangle_{\hat{r}}$ state and $|^3L'_J\rangle_{\hat{r}}$ states, respectively, which are defined as

$$|^3L_J\rangle_{\hat{r}} = |1,1\rangle_s Y_{L,L}(\hat{r}), \tag{29}$$

$$|^3L'_J\rangle_{\hat{r}} = \sum_{m_s} C_{m_s}|1,m_s\rangle_s Y_{L+2,L+1-m_s}(\hat{r}). \tag{30}$$

For S-D mixed states, we have the following sets of equations:

$$\frac{2}{\pi R^3}\Delta a_i a_i^2 N_{li}^2\left(\sqrt{\left(\frac{a_i}{R}\right)^2+m_Q^2}+\sqrt{\left(\frac{a_i}{R}\right)^2+m_{\bar{q}}^2}\right)c_i^{(1)} + \sum_{j=1}^{N}\frac{a_j}{N_{li}^2 a_i}\int_0^R \mathrm{d}r\langle V\rangle_{11}r^2 j_l\left(\frac{a_i r}{R}\right)j_l\left(\frac{a_j r}{R}\right)c_j^{(1)} + \sum_{j=1}^{N}\frac{a'_j}{N_{li}^2 a_i}\int_0^R \mathrm{d}r\langle V\rangle_{12}r^2 j_l\left(\frac{a_i r}{R}\right)j_{l'}\left(\frac{a'_j r}{R}\right)c_j^{(2)}=Ec_i^{(1)}, \tag{31}$$

$$\frac{2}{\pi R^3}\Delta a'_i a'^2_i N_{l'i}^2\left(\sqrt{\left(\frac{a'_i}{R}\right)^2+m_Q^2}+\sqrt{\left(\frac{a'_i}{R}\right)^2+m_{\bar{q}}^2}\right)c_i^{(2)} + \sum_{j=1}^{N}\frac{a_j}{N_{l'i}^2 a'_i}\int_0^R \mathrm{d}r\langle V\rangle_{21}r^2 j_{l'}\left(\frac{a'_i r}{R}\right)j_l\left(\frac{a_j r}{R}\right)c_j^{(1)} + \sum_{j=1}^{N}\frac{a'_j}{N_{l'i}^2 a'_i}\int_0^R \mathrm{d}r\langle V\rangle_{22}r^2 j_{l'}\left(\frac{a'_i r}{R}\right)j_{l'}\left(\frac{a'_j r}{R}\right)c_j^{(2)}=Ec_i^{(2)}. \tag{32}$$

These equations can be used to define the Hamiltonian matrix H in terms of four $N\times N$ matrices H_{11}, H_{12}, H_{21}, and H_{22}. Note that for S-D mixed states, contributions to $\langle V\rangle_{12}$ and $\langle V\rangle_{21}$ are from the tensor operator of the potential.

Our numerical results also depend on the order of the matrix N. For a large value of N, dependency is negligible. In our calculations, we take N = 50 and R = 25 GeV^{-1}. Numerical values of quark masses and other parameters of the conventional potential model are extracted from fitting the spectrum to experimentally known states. We used 14 experimentally well-established states for fitting. The states that we used for fitting parameter values are given in Table 2. For spectrum fitting, we used differential evolution (DE) [46]. DE is a stochastic global optimization algorithm. In multiple independent trials, DE consistently converged to the global minimum of the objective function. By minimizing the χ^2 function using the DE algorithm, we determined the best parameter fits. Our fitted parameter values were m_c = 1.47 ± 0.01 GeV, $m_{u/d}$ = 0.020 ± 0.001 GeV, $\tilde{m}_{u/d}$ = 0.430 ± 0.001 GeV, m_s = 0.336 ± 0.007 GeV, $\tilde{m}_s$ = 0.5967 ± 0.00046 GeV, α_s^c = 0.240 ± 0.025, b = 0.211 ± 0.002 GeV^2, c = –0.4321 ± 0.0041 GeV, σ_0 = 0.5221 ± 0.013 GeV, s_0 = 0.91 ± 0.15, ϵ_2 = 1.5 ± 0.59, ϵ_3 = 1.5 ± 0.1, and ϵ_4= 1.31 ± 0.14. Our predicted spectra for conventional charmed and charmed strange mesons are shown in Figs. 2 and 3. In Figs. 4 and 5, we present our calculated spectra of hybrid charmed mesons and hybrid charmed strange mesons. Comparisons of our calculated spectra for conventional D and D_s mesons with those of other studies are presented in Tables 2 and 3.

V. RADIATIVE TRANSITIONS

Radiative transitions play a vital role in the identification of meson states. The $E1$ radiative partial width between initial and final mesons in the non-relativistic quark model is given by [55]

$$\begin{aligned}&\Gamma(n^{2S+1}L_J\to n'^{2S'+1}L'_{J'}+\gamma)\\&=\frac{4}{3}\langle e_Q\rangle^2\alpha\omega^3C_{fi}\delta_{SS'}\delta_{L,L'\pm1}|\langle n'^{2S'+1}L'_{J'}|r|n^{2S+1}L_J\rangle|^2\frac{E_f}{M_i},\end{aligned}\tag{33}$$

where $\alpha=\dfrac{1}{137}$ is the electromagnetic fine structure constant, ω is photon energy, $|n^{2S+1}L_J\rangle$ is the initial meson state, $|n'^{2S'+1}L'_{J'}\rangle$ is the final meson state, E_f is the energy of final meson state, and M_i is the mass of the initial meson. C_{fi} is the angular momentum matrix element and is defined as

$$C_{fi}=\max(L,L')(2J'+1)\begin{Bmatrix}L' & J' & S\\ J & L & 1\end{Bmatrix}^2,$$

where $\begin{Bmatrix}\cdot & \cdot & \cdot\\ \cdot & \cdot & \cdot\end{Bmatrix}$ is a 6-j symbol. In Eq. (33), $\langle e_Q\rangle$ is

$$\langle e_Q\rangle=\frac{m_ce_q-m_qe_{\bar{c}}}{m_q+m_c}.\tag{34}$$

Here, m_c and m_q are the constituent masses of the charm

Table 2. Comparison of our calculated spectrum (in MeV) for the conventional D and D_s mesons with those of other studies.

Meson	J^P	Our Mass Results	GI Model [20]	[22]	[39]	PDG [18]
		Charmed strange mesons:				
$D_s^\pm$	0^-	2001.36	1979	1963	1964	1968.35 ± 0.07
$D_s^{*\pm}$	1^-	2079.63	2129	2103	2102	2112.2 ± 0.4
$D_{s1}(2536)^\pm$	1^+	2535.92	2556	2533	2510	2535.11 ± 0.06
$D_{s2}^*(2573)$	2^+	2569.18	2592	2573	2548	2569.1 ± 0.8
$D_{s1}^*(2700)^\pm$	1^-	2706.22	2732	2709	2680	2714 ± 5
$D_{s1}^*(2860)^\pm$	1^-	2820.59	2899	2803	2771	2859 ± 27 [47, 48]
$D_{s3}^*(2860)^\pm$	3^-	2869.84	2917	2853	2816	2860 ± 7
		Charmed mesons:				
D^0	0^-	1890.66	1877	1867		1864.83 ± 0.05
$D^*(2007)^0$	1^-	1980.63	2041	2004		2006.85 ± 0.05
$D_0^*(2300)^0$	0^+	2334.64	2399	2302		2343 ± 10
$D_1(2430)^0$	1^+	2458.56	2456	2415		2412 ± 9
$D_1(2420)^0$	1^+	2391.87	2467	2429		2422.1 ± 0.6
$D_2^*(2460)^0$	2^+	2464.39	2502	2468		$2461.1^{+0.7}_{-0.8}$
$D_3^*(2750)$	3^-	2789.59	2833	2754		2763.1 ± 3.2

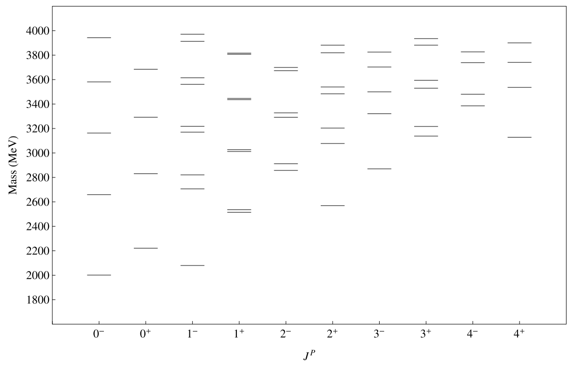

Fig. 3. Conventional charmed strange mesons spectrum.

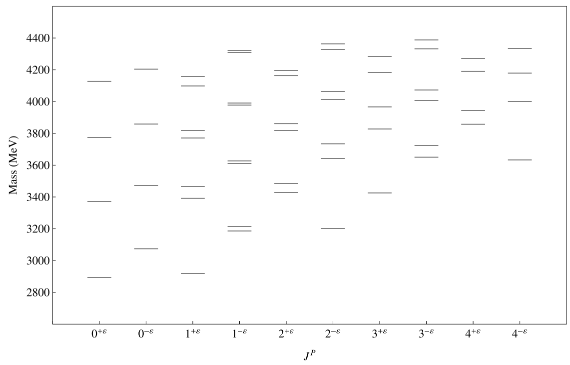

Fig. 5. Hybrid charmed strange mesons spectrum.

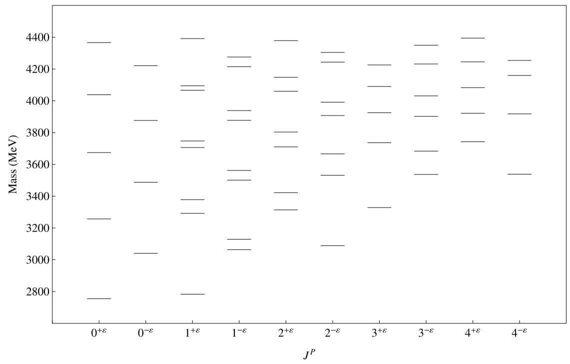

Fig. 4. Hybrid charmed mesons spectrum.

and light (q) quarks, respectively. For the D meson, q = u/d and for the D_s meson, $q = s$. $e_{\bar{c}} = -2/3$ is the electric charge of the anti-charm quark in units of $|e|$. $e_u = +2/3$, $e_d = -1/3$, and $e_s = -1/3$ are electric charges of up, down, and strange quarks, respectively, in units of $|e|$.

Matrix elements $\langle n'^{2S'+1}L'_{J'}|r|n^{2S+1}L_J\rangle$ are calculated using the relativistic quark model wave functions obtained in Section IV. In $E1$ transitions, relativistic corrections are implicitly included due to the contribution of spin dependent interactions in the Hamiltonian.

The *M1* radiative partial width of the *S*-wave meson bound state is [20]

$$\Gamma(n^{2S+1}L_J \to n'^{2S'+1}L_{J'}+\gamma) = \frac{\alpha}{3}\omega^3(2J'+1)\delta_{S,S'\pm1}|\langle f|\frac{e_q}{m_q}j_0\left(\frac{m_c}{m_q+m_c}\omega r\right) - \frac{e_{\bar{c}}}{m_c}j_0\left(\frac{m_q}{m_q+m_c}\omega r\right)|i\rangle|^2, \tag{35}$$

where j_0 is the spherical Bessel function. Electromagnetic transitions are sensitive to the internal structure of mesons, particularly in the case of mixed states. A mixed state is a linear combination of two states; only the component(s) that satisfy the selection rules for *E1* and *M1* transitions contribute to the transition amplitude. To calculate the decay width of *M1* transitions for conventional S-wave meson bound states, the M1 selection rules and Eq. (28) imply that only the $1^- \leftrightarrow 0^-$ transition is allowed. Furthermore, only the $^3S_1$ component of the 1^- state contributes to the decay width. To calculate the decay width of $E1$ transitions of conventional meson bound states ($L<3$), the selection rules of $E1$ transitions and Eqs. (22, 28) indicate that only four transitions contribute, *i.e.*, $1^+ \leftrightarrow 0^-$, $1^- \leftrightarrow 0^+$, $1^- \leftrightarrow 1^+$, and $2^- \leftrightarrow 1^+$. In the $1^+ \leftrightarrow 0^-$ transition, only the $^1P_1$ component of the 1^+ state fulfil the selection rule of the $E1$ transitions. In the $1^- \leftrightarrow 0^+$ transition, both the components of the 1^- state have contributions. For the $1^- \leftrightarrow 1^+$ transition, both components of

Table 3. Comparison of our calculated spectrum (in MeV) for conventional D and D_s mesons with those of other studies and experimental data.

Meson	J^P	Our Results	GI Model [20]	[22]	[39]	Exp. Data
		Charmed strange mesons:				
$D^*_{s0}(2590)^+$	0^-	2659	2673	2582	2557	2591±9 [49]
$D^*_{sJ}(3040)^\pm$	1^+, 2^+	3026.94, 3077.36				3044^{+31}_{-9} [48]
		Charmed mesons:				
$D_0(2550)^0$	0^-	2553.34	2581	2483		2549 ± 19 [50, 51]
$D^*_1(2600)^0$	1^-	2618.66	2643	2613		2627 ± 10 [51, 52]
$D_2(2740)^0$	2^-	2752.03	2816	2737		2747 ± 6 [50, 53]
$D^*_1(2760)^0$	1^-	2770.32	2817	2785		2781 ± 22 [54]
$D(3000)^0$	3^+, 3^-, 4^-	3184.76, 3233.29, 3275.27				3214 ± 60 [52, 53]

Table 4. Calculated conventional D and D_s meson masses (in MeV) for $J^P = 0^-, 0^+, 1^-, 1^+, 2^-, 2^+, 3^-, 3^+, 4^-$, and 4^+.

J^P	n	D Meson	D_s Meson
0^-	1	1890.66	2001.36
	2	2553.34	2659.00
	3	3070.94	3162.90
	4	3491.35	3581.01
0^+	1	2334.64	2221.26
	2	2895.60	2830.25
	3	3339.03	3292.43
	4	3723.79	3684.70
1^-	1	1980.63	2079.63
	2	2618.66	2706.22
	3	2770.32	2820.59
	4	3111.91	3170.35
	5	3210.21	3218.06
	6	3524.85	3561.34
	7	3599.51	3614.62
	8	3888.75	3912.91
1^+	1	2391.87	2514.83
	2	2458.56	2535.92
	3	2880.36	3012.05
	4	2955.80	3026.94
	5	3327.55	3435.81
	6	3400.51	3446.24
	7	3710.89	3807.50
	8	3784.40	3816.56
2^-	1	2752.03	2857.35
	2	2862.13	2911.54
	3	3188.32	3292.05
	4	3287.53	3327.83
	5	3571.28	3672.60
	6	3666.60	3699.38
	7	3916.99	4014.94
	8	4008.79	4037.37
2^+	1	2464.39	2569.18
	2	2959.26	3077.36
	3	3131.47	3203.58
	4	3379.56	3483.48
	5	3494.62	3539.61
	6	3750.46	3819.04
	7	3840.78	3881.70
	8	4086.20	4130.11

Continued on next column

Table 4-continued from previous column

J^P	n	D Meson	D_s Meson
3^-	1	2789.59	2869.84
	2	3233.29	3320.75
	3	3448.43	3499.65
	4	3615.56	3702.96
	5	3765.23	3825.09
	6	3959.01	4053.21
	7	4075.86	4114.68
	8	4274.05	4363.43
3^+	1	3031.60	3138.04
	2	3184.76	3216.67
	3	3427.33	3529.81
	4	3560.11	3594.36
	5	3781.48	3881.76
	6	3904.52	3935.16
	7	4105.19	4203.53
	8	4222.14	4248.79
4^-	1	3275.27	3385.16
	2	3466.85	3480.50
	3	3634.65	3738.40
	4	3804.95	3826.51
	5	3971.98	4073.56
	6	4125.85	4149.44
	7	4278.55	4376.37
	8	4424.86	4445.97
4^+	1	3050.12	3128.49
	2	3460.14	3536.36
	3	3727.59	3740.77
	4	3819.37	3900.19
	5	4021.00	4050.96
	6	4144.89	4230.53
	7	4303.97	4357.16
	8	4445.31	4534.66

the initial and final states contribute except the $^1P_1$ component of the 1^+ state. Finally, in the $2^- \leftrightarrow 1^+$ transition, both components of the initial and final states contribute.

VI. RESULTS AND CONCLUSIONS

In this work, we present a detailed spectrum of conventional and hybrid charmed and charmed strange mesons. States with the same J^P quantum numbers are treated as mixed states. We have incorporated both spin and S-D mixing through the off-diagonal matrix ele-

Table 5. Calculated hybrid D and D_s meson masses (in MeV) for $J^P = 0^{-\varepsilon}, 0^{+\varepsilon}, 1^{-\varepsilon}, 1^{+\varepsilon}, 2^{-\varepsilon}, 2^{+\varepsilon}, 3^{-\varepsilon}, 3^{+\varepsilon}, 4^{-\varepsilon}$, and $4^{+\varepsilon}$.

J^P	n	Hybrid D Meson	Hybrid D_s Meson
$0^{+\varepsilon}$	1	2755.01	2894.34
	2	3256.86	3371.39
	3	3674.27	3773.52
	4	4038.16	4128.21
$0^{-\varepsilon}$	1	3040.45	3073.69
	2	3487.44	3471.19
	3	3876.36	3858.93
	4	4220.98	4204.41
$1^{+\varepsilon}$	1	2783.31	2917.32
	2	3291.98	3392.35
	3	3377.88	3467.12
	4	3705.86	3771.09
	5	3747.28	3818.40
	6	4066.32	4098.38
	7	4094.33	4159.38
	8	4391.27	4406.70
$1^{-\varepsilon}$	1	3063.57	3186.10
	2	3129.03	3214.35
	3	3501.03	3610.14
	4	3561.83	3626.80
	5	3877.47	3978.27
	6	3938.51	3991.02
	7	4214.71	4309.78
	8	4275.42	4320.49
$2^{+\varepsilon}$	1	3313.71	3429.11
	2	3422.03	3484.54
	3	3710.06	3817.38
	4	3803.52	3860.47
	5	4060.25	4162.55
	6	4148.00	4196.43
	7	4378.76	4476.95
	8	4462.95	4504.55
$2^{-\varepsilon}$	1	3088.68	3202.11
	2	3531.70	3642.38
	3	3666.11	3734.10
	4	3907.27	4012.51
	5	3991.32	4062.51
	6	4243.29	4329.07
	7	4304.42	4363.03
	8	4550.91	4612.00

Continued on next column

Table 5-continued from previous column

J^P	n	Hybrid D Meson	Hybrid D_s Meson
$3^{+\varepsilon}$	1	3328.26	3425.32
	2	3736.37	3827.75
	3	3924.76	3966.53
	4	4089.99	4182.79
	5	4225.45	4284.57
	6	4409.37	4503.65
	7	4512.24	4572.02
	8	4703.77	4797.78
$3^{-\varepsilon}$	1	3536.73	3650.73
	2	3683.47	3723.53
	3	3902.08	4008.45
	4	4030.85	4073.06
	5	4231.61	4331.70
	6	4349.85	4387.91
	7	4534.57	4619.30
	8	4645.99	4671.07
$4^{+\varepsilon}$	1	3742.56	3858.08
	2	3921.79	3943.51
	3	4082.66	4191.13
	4	4244.97	4271.20
	5	4394.41	4497.79
	6	4544.24	4572.21
	7	4683.88	4783.46
	8	4824.56	4852.37
$4^{-\varepsilon}$	1	3538.36	3633.01
	2	3917.60	4000.87
	3	4159.43	4179.46
	4	4254.05	4335.09
	5	4446.62	4483.56
	6	4560.83	4641.67
	7	4715.93	4763.97
	8	4845.22	4927.05

ments of the Hamiltonian. In Figs. 2 to 5, state mixing phenomena are explicitly visualized by the spectrum pattern. Ref. [20] includes spin mixing effects, although S-D mixing is ignored in the calculations therein. In Ref. [22], the spin dependent Hamiltonian part is added perturbatively after solving the eigenequation. In this study, we use the complete Hamiltonian, including the spin dependent part, in the eigenvalue equation. This approach enables us to study both spin effects and S-D mixing without resorting to perturbation theory.

Our calculated spectrum of conventional D and D_s

mesons is reported in Table 4 with increasing mass. n is the number of eigenvalues associated with a specific value of J^P. For unmixed states, the 0^+ ($^3P_0$) states have a larger mass than the 0^- ($^1S_0$) states due to spin and orbital excitation. For S-D mixed states, higher orbital excited states (*e.g.*, 2^+, $^3P_2 \leftrightarrow {}^3F_2$) have larger masses than lower excited states (*e.g.*, 1^-, $^3S_1 \leftrightarrow {}^3D_1$). The same is observed for the spin singlet and spin triplet mixed states. States with higher orbital excitations (*e.g.*, 2^-, $^1D_2 \leftrightarrow {}^3D_2$) have larger masses than lower orbital excited states (*e.g.*, 1^+, $^1P_1 \leftrightarrow {}^3P_1$). We also compare our calculated spectrum of conventional D and D_s mesons with experimental results and the results of other studies in Tables 2 and 3. Our results show good agreement with both previous study findings and experimental data. We used meson states in Table 2 for fitting the parameter values. Table 3 shows the efficiency of our results. In Table 3, we identify $D^*_{sJ}(3040)^{\pm}$ and $D(3000)^0$ as the 1^+ and 3^- states, respectivley. We tentatively identify $D^*_{sJ}(3040)^{\pm}$ and $D(3000)^0$ as the 2^+ and 3^+ states, respectively. $D(3000)^0$ could be considered the 4^- state. Because the nature of the $D^*_{s0}(2317)^{\pm}$ and $D_{s1}(2460)^{\pm}$ states is unclear, as discussed in Section I, we did not include these states in the fitting procedure. Moreover, we did not find any good matches for these states in either the conventional or hybrid mass spectrum. This result is consistent with the previously suggested exotic nature of $D^*_{s0}(2317)$ and $D_{s1}(2460)$ mesons.

In Table 5, we report the computed masses of hybrid D and D_s mesons. For hybrid candidates, the parity condition differs from that of conventional mesons owing to the contribution of the excited gluonic field, as discussed in Section I. It is observed that hybrid states have greater masses compared to conventional mesons. This occurs due to gluonic excitations in Π_u states. In Tables 6 and 7, we report our calculated $E1$ transitions for conventional to conventional and hybrid to hybrid mesons, respectively. We also present $M1$ transitions for conventional to conventional and hybrid to hybrid mesons in Tables 8 and 9, respectively. We observed that the decay width of $D^0(c\bar{u})$ states is larger than that of $D^{\pm}(c\bar{d})$ states, except for few states in $M1$ transitions. In Table 10, we compare our calculated radiative decay width of conventional mesons with those of other studies and experimental results. Our results are consistent with those of other studies except for those corresponding to a few D^0 meson states. We expect our predicted results to be useful for the detection of new charmed and charmed strange mesons.

Table 6. Partial widths of the $E1$ decays (in keV) of conventional D and D_s mesons.

Transition	Initial state nJ^P	Final state nJ^P	Γ_{e1} (D meson) ($c\bar{u}$, $c\bar{d}$)	Γ_{e1} (D_s meson)
$0^- \to 1^+\gamma$	20^-	11^+	91.149, 3.457	0.4176
		21^+	75.435, 1.9573	0.2435
	30^-	11^+	210.5, 5.8748	0.3448
		21^+	226.65, 5.8811	0.2216
		31^+	432.72, 11.228	1.049
		41^+	109.09, 2.8305	0.697
$0^+ \to 1^-\gamma$	10^+	11^-	728.01, 19.4031	0.0859
	20^+	11^-	184.37, 4.8241	2.0001
		21^-	545.88, 14.164	0.2027
		31^-	35.948, 0.9328	0.0002
	30^+	11^-	47.770, 1.2456	0.3441
		21^-	290.88, 7.5475	1.6971
		31^-	407.65, 10.577	1.6964
		41^-	748.15, 19.413	0.5871
		51^-	158.37, 4.1092	0.162
$1^- \to 0^+\gamma$	21^-	10^+	43.527, 1.1612	1.9786
	31^-	10^+	628.92, 16.779	3.8272
	41^-	10^+	776.18, 20.707	0.1186
		20^+	604.83, 16.136	2.8181
	51^-	10^+	49.96, 1.3328	0.2344
		20^+	604.83, 16.136	2.8181

Continued on next page

Table 6-continued from previous page

Transition	Initial state nJ^P	Final state nJ^P	$\Gamma_{e1}(D$ meson) $(c\bar{u},\ c\bar{d})$	$\Gamma_{e1}(D_s$ meson)
$1^- \to 1^+\gamma$	21^-	11^+	82.384, 2.7702	0.4364
		21^+	73.119, 1.8973	0.291
	31^-	11^+	497.36, 14.921	1.6613
		21^+	463.44, 12.025	1.263
	41^-	11^+	1028.9, 28.573	0.9155
		21^+	1016.9, 26.386	0.5979
		31^+	383.55, 9.9521	0.6226
		41^+	133.93, 3.4751	0.4148
	51^-	11^+	234.27, 6.4414	0.5734
		21^+	244.65, 6.3481	0.3518
		31^+	1126.6, 29.234	1.1176
		41^+	585.33, 15.188	0.7807
$1^+ \to 0^-\gamma$	11^+	10^-	847.18, 20.415	3.4365
	21^+	10^-	886.97, 23.498	3.7954
	31^+	10^-	0.123, 0.0032	0.1012
		20^-	443.01, 11.495	2.1211
	41^+	10^-	0.7203, 0.0189	0.0009
		20^-	764.76, 19.844	2.7341
$1^+ \to 1^-\gamma$	11^+	11^-	638.97, 14.809	2.2145
	21^+	11^-	851.13, 22.510	2.526
	31^+	11^-	80.893, 2.1169	0.4596
		21^-	313.77, 8.1415	1.8567
		31^-	4.6457, 0.1205	0.3447
	41^+	11^-	106.76, 2.7914	0.5276
		21^-	622.18, 16.144	2.2821
		31^-	20.975, 0.5442	0.4659
$1^+ \to 2^-\gamma$	31^+	12^-	65.085, 1.6888	0.5529
		22^-	0.2119, 0.0055	0.1558
	41^+	12^-	238.29, 6.1831	0.8464
		22^-	26.278, 0.6818	0.2738
	51^+	12^-	1.3736, 0.0356	0.1362
		22^-	5.0118, 0.13	0.1717
		32^-	181.45, 4.7082	0.998
		42^-	5.0814, 0.1318	0.4126
	61^+	12^-	2.6022, 0.0675	0.2015
		22^-	0.6375, 0.0165	0.2359
		32^-	554.7, 14.393	1.3456
		42^-	99.485, 2.5814	0.5961
$2^- \to 1^+\gamma$	12^-	11^+	1324.5, 40.073	5.3991
		21^+	1235.9, 32.0705	4.27
	22^-	11^+	2821.6, 81.961	8.0433

Continued on next page

Table 6-continued from previous page

Transition	Initial state nJ^P	Final state nJ^P	Γ_{e1} (D meson) ($c\bar{u}$, $c\bar{d}$)	Γ_{e1} (D_s meson)
		21^+	2692.4, 69.861	6.5345
	32^-	11^+	135.6, 3.736	0.0116
		21^+	154.87, 4.0186	0.0318
		31^+	1541.9, 40.008	4.8947
		41^+	746.69, 19.375	3.7323
	42^-	11^+	167.93, 4.589	0.0259
		21^+	194.43, 5.045	0.0352
		31^+	3316.8, 86.062	6.8996
		41^+	2019.9, 52.411	5.3872

Table 7. Partial widths of the $E1$ decays (in keV) of hybrid D and D_s mesons.

Transition	Initial state nJ^P	Final state nJ^P	Γ_{e1} (hybrid D meson) ($c\bar{u}$, $c\bar{d}$)	Γ_{e1} (hybrid D_s meson)
$0^{+\varepsilon} \to 1^{-\varepsilon}\gamma$	$20^{+\varepsilon}$	$11^{-\varepsilon}$	261.12, 6.7754	1.059
		$21^{-\varepsilon}$	81.811, 2.1228	0.6407
	$30^{+\varepsilon}$	$11^{-\varepsilon}$	57.046, 1.4802	0.2516
		$21^{-\varepsilon}$	60.926, 1.5809	0.2588
		$31^{-\varepsilon}$	385.99, 10.016	1.5485
		$41^{-\varepsilon}$	117.44, 3.0472	1.0873
$0^{-\varepsilon} \to 1^{+\varepsilon}\gamma$	$10^{-\varepsilon}$	$11^{+\varepsilon}$	618.71, 16.054	0.4149
	$20^{-\varepsilon}$	$11^{+\varepsilon}$	387.02, 10.0423	1.9049
		$21^{+\varepsilon}$	264.43, 6.8614	0.0996
		$31^{+\varepsilon}$	63.071, 1.6365	0.00002
	$30^{-\varepsilon}$	$11^{+\varepsilon}$	6.5882, 0.1709	0.2337
		$21^{+\varepsilon}$	251.11, 6.5156	1.8328
		$31^{+\varepsilon}$	153.29, 3.9775	2.48
		$41^{+\varepsilon}$	301.26, 7.817	0.3068
		$51^{+\varepsilon}$	158.79, 4.1204	0.0377
$1^{+\varepsilon} \to 0^{-\varepsilon}\gamma$	$21^{+\varepsilon}$	$10^{-\varepsilon}$	199.35, 5.3184	1.3168
	$31^{+\varepsilon}$	$10^{-\varepsilon}$	511.52, 13.646	2.395
	$41^{+\varepsilon}$	$10^{-\varepsilon}$	3.2826, 0.0876	0.0766
		$20^{-\varepsilon}$	231.81, 6.1844	2.0572
	$51^{+\varepsilon}$	$10^{-\varepsilon}$	16.243, 0.4333	0.2632
		$20^{-\varepsilon}$	417.04, 11.126	2.48
$1^{+\varepsilon} \to 1^{-\varepsilon}\gamma$	$21^{+\varepsilon}$	$11^{-\varepsilon}$	222.27, 5.7673	0.7543
		$21^{-\varepsilon}$	85.868, 2.2281	0.4825
	$31^{+\varepsilon}$	$11^{-\varepsilon}$	436.29, 11.3207	1.7273
		$21^{-\varepsilon}$	229.88, 5.9648	1.2476
	$41^{+\varepsilon}$	$11^{-\varepsilon}$	71.744, 1.8616	0.4743
		$21^{-\varepsilon}$	61.15, 1.5867	0.3914
		$31^{-\varepsilon}$	303.65, 7.8791	0.8211

Continued on next page

Table 7-continued from previous page

Transition	Initial state nJ^P	Final state nJ^P	Γ_{e1} (hybrid D meson) ($c\bar{u}$, $c\bar{d}$)	Γ_{e1} (hybrid D_s meson)
		$41^{-\varepsilon}$	115.48, 2.9963	0.5718
	$51^{+\varepsilon}$	$11^{-\varepsilon}$	132.82, 3.4463	0.1873
		$21^{-\varepsilon}$	113.01, 2.9322	0.156
		$31^{-\varepsilon}$	374.27, 9.7114	1.452
		$41^{-\varepsilon}$	174.23, 4.5208	1.0843
$1^{-\varepsilon} \to 0^{+\varepsilon}\gamma$	$11^{-\varepsilon}$	$10^{+\varepsilon}$	420.74, 10.917	1.4283
	$21^{-\varepsilon}$	$10^{+\varepsilon}$	714.93, 18.551	1.8474
	$31^{-\varepsilon}$	$10^{+\varepsilon}$	21.638, 0.5615	0.000008
		$20^{+\varepsilon}$	350.18, 9.0864	1.3169
	$41^{-\varepsilon}$	$10^{+\varepsilon}$	23.361, 0.6062	0.0033
		$20^{+\varepsilon}$	652.03, 16.918	1.6334
$1^{-\varepsilon} \to 1^{+\varepsilon}\gamma$	$11^{-\varepsilon}$	$11^{+\varepsilon}$	462.52, 12.001	1.4309
	$21^{-\varepsilon}$	$11^{+\varepsilon}$	827.38, 21.468	1.8929
	$31^{-\varepsilon}$	$11^{+\varepsilon}$	163.51, 4.2426	0.5119
		$21^{+\varepsilon}$	265.17, 6.8805	1.2207
		$31^{+\varepsilon}$	49.942, 1.2959	0.473
	$41^{-\varepsilon}$	$11^{+\varepsilon}$	196.41, 5.0965	0.577
		$21^{+\varepsilon}$	543.57, 14.104	1.5197
		$31^{+\varepsilon}$	158.73, 4.1187	0.6515
$1^{-\varepsilon} \to 2^{+\varepsilon}\gamma$	$31^{-\varepsilon}$	$12^{+\varepsilon}$	251.90, 6.5361	1.0387
		$22^{+\varepsilon}$	22.292, 0.5784	0.3843
	$41^{-\varepsilon}$	$12^{+\varepsilon}$	549.57, 14.26	1.3888
		$22^{+\varepsilon}$	116.31, 3.0179	0.5716
	$51^{-\varepsilon}$	$12^{+\varepsilon}$	12.435, 0.3227	0.0632
		$22^{+\varepsilon}$	30.026, 0.7791	0.1367
		$32^{+\varepsilon}$	377.98, 9.8075	1.5399
		$42^{+\varepsilon}$	38.496, 0.9989	0.6371
	$61^{-\varepsilon}$	$12^{+\varepsilon}$	1.709, 0.0443	0.0708
		$22^{+\varepsilon}$	18.596, 0.4825	0.1541
		$32^{+\varepsilon}$	860.24, 22.321	2.0341
		$42^{+\varepsilon}$	211.48, 5.4873	0.9093
$2^{+\varepsilon} \to 1^{-\varepsilon}\gamma$	$12^{+\varepsilon}$	$11^{-\varepsilon}$	872.62, 22.642	3.3811
		$21^{-\varepsilon}$	373.06, 9.6801	2.3478
	$22^{+\varepsilon}$	$11^{-\varepsilon}$	2390.7, 62.033	6.0388
		$21^{-\varepsilon}$	1386.2, 35.968	4.5079
	$32^{+\varepsilon}$	$11^{-\varepsilon}$	74.05, 1.9214	0.0924
		$21^{-\varepsilon}$	74.711, 1.9386	0.0787
		$31^{-\varepsilon}$	736, 19.097	3.0566
		$41^{-\varepsilon}$	284.58, 7.3841	2.3242
	$42^{+\varepsilon}$	$11^{-\varepsilon}$	57.592, 1.4944	0.0451
		$21^{-\varepsilon}$	66.767, 1.7324	0.0386

Continued on next page

Table 7-continued from previous page

Transition	Initial state nJ^P	Final state nJ^P	Γ_{e1} (hybrid D meson) ($c\bar{u}$, $c\bar{d}$)	Γ_{e1} (hybrid D_s meson)
		$31^{-\varepsilon}$	2063.6, 53.545	5.1521
		$41^{-\varepsilon}$	1143.8, 29.679	4.0959

Table 8. Partial widths of the $M1$ decays (in keV) of conventional D and D_s mesons.

Transition	Initial state nJ^P	Final state nJ^P	Γ_{m1} (D meson) ($c\bar{u}$, $c\bar{d}$)	Γ_{m1} (D_s meson)
$0^- \to 1^-\gamma$	20^-	11^-	11.097, 7.4747	2.184
	30^-	11^-	0.1487, 6.2222	2.3694
		21^-	22.198, 10.062	2.9894
		31^-	98.771, 1.2647	0.209
	40^-	11^-	0.1319, 1.566	0.5123
		21^-	25.08, 18.489	5.9304
		31^-	248.86, 10.857	0.1343
		41^-	16.733, 7.8301	3.7441
		51^-	68.052, 0.0079	2.0575
$1^- \to 0^-\gamma$	11^-	10^-	23.648, 0.6064	0.0665
	21^-	10^-	127.55, 17.5012	4.0203
		20^-	2.5479, 0.0644	0.0042
	31^-	10^-	2085, 19.985	7.9164
		20^-	4.8418, 0.19	0.0919
	41^-	10^-	112.9, 17.719	1.622
		20^-	82.281, 10.879	1.9332
		30^-	0.6405, 0.0163	0.00001
	51^-	10^-	1350, 0.9538	5.1259
		20^-	42.254, 1.3827	2.8697
		30^-	7.1297, 0.123	0.004

Table 9. Partial widths of the $M1$ decays (in keV) of hybrid D and D_s mesons.

Transition	Initial state nJ^P	Final state nJ^P	Γ_{m1} (hybrid D meson) ($c\bar{u}$, $c\bar{d}$)	Γ_{m1} (hybrid D_s meson)
$0^{+\varepsilon} \to 1^{+\varepsilon}\gamma$	$20^{+\varepsilon}$	$11^{+\varepsilon}$	22.206, 9.4979	2.1082
	$30^{+\varepsilon}$	$11^{+\varepsilon}$	8.4751, 10.6	2.2568
		$21^{+\varepsilon}$	14.759, 6.9874	2.1905
		$31^{+\varepsilon}$	2.6918, 1.303	0.5497
	$40^{+\varepsilon}$	$11^{+\varepsilon}$	9.428, 5.1214	0.7265
		$21^{+\varepsilon}$	21.874, 16.759	4.8863
		$31^{+\varepsilon}$	13.313, 3.7718	0.6848
		$41^{+\varepsilon}$	12.489, 5.5476	2.5828
		$51^{+\varepsilon}$	10.924, 2.235	1.2671
$1^{+\varepsilon} \to 0^{+\varepsilon}\gamma$	$11^{+\varepsilon}$	$10^{+\varepsilon}$	0.2161, 0.0056	0.0003
	$21^{+\varepsilon}$	$10^{+\varepsilon}$	53.308, 7.458	1.1989
		$20^{+\varepsilon}$	0.4085, 0.0105	0.0002

Continued on next page

Table 9-continued from previous page

Transition	Initial state nJ^P	Final state nJ^P	Γ_{m1} (hybrid D meson) ($c\bar{u}$, $c\bar{d}$)	Γ_{m1} (hybrid D_s meson)
	$31^{+\varepsilon}$	$10^{+\varepsilon}$	425.28, 17.191	2.2738
		$20^{+\varepsilon}$	12.745, 0.2962	0.0171
	$41^{+\varepsilon}$	$10^{+\varepsilon}$	60.381, 11.716	0.9809
		$20^{+\varepsilon}$	46.49, 6.0773	0.9054
	$51^{+\varepsilon}$	$10^{+\varepsilon}$	760.03, 29.874	2.861
		$20^{+\varepsilon}$	234.39, 9.8806	1.5053
		$30^{+\varepsilon}$	2.5875, 0.0632	0.0022

Table 10. Comparison of our calculated radiative decay partial widths (in keV) with those of other studies. D_1 and D_1' are the mixed states ($J^P = 1^+$) of charmed mesons.

Mode	Our Results	GI Model [20]	[56]	[57]	[39]	PDG [18]
			Charmed strange mesons			
$D_s^{*\pm} \to D_s^{\pm}\gamma$	0.0665	1.03	2.39	1.12		< 1776.5
$D_{s1}(2536)^{\pm} \to D_s^{\pm}\gamma$	3.7954	9.23	61.2	37.7	3.53	
$D_{s1}(2536)^{\pm} \to D_s^{*\pm}\gamma$	2.526	9.61	9.21	5.74	4.74	
			Charmed mesons ($c\bar{u}$)			
$D^*(2007)^0 \to D^0\gamma$	23.648	106				< 741
$D_0^*(2300)^0 \to D^*(2007)^0\gamma$	728.01	288				
$D_1(2430)^0 \to D^0\gamma$	847.18	640				
$D_1(2420) \to D^0\gamma$	886.97	156				
$D_1(2430)^0 \to D^*(2007)^0\gamma$	638.97	82.8				
$D_1(2420) \to D^*(2007)^0\gamma$	851.13	386				
			Charmed mesons ($c\bar{d}$)			
$D^*(2010)^{\pm} \to D^{\pm}\gamma$	0.6064	10.8				≈ 1.334
$D_0^* \to D^*(2010)^{\pm}\gamma$	19.4031	30				
$D_1 \to D^{\pm}\gamma$	20.415	66				
$D_1' \to D^{\pm}\gamma$	23.498	16.1				
$D_1 \to D^*(2010)^{\pm}\gamma$	14.809	8.6				
$D_1' \to D^*(2010)^{\pm}\gamma$	22.51	39.9				

References

[1] G.M. Beladidze, *et al* (VES Collaboration), Phys. Lett. B **313**, 276 (1993)
[2] K. J. Juge, J. Kuti, and C. J. Morningstar, Nucl. Phys. Proc. Suppl. **63**, 326 (1998)
[3] K. J. Juge, J. Kuti, and C. J. Morningstar, AIP Conf. Proc. **688**, 193 (2003)
[4] K. J. Juge, J. Kuti, and C. J. Morningstar, Phys. Rev. Lett. **82**, 4400 (1999)
[5] S. Capitani, O. Philipsen, C. Reisinger *et al.*, Phys. Rev. D **99**, 034502 (2019)
[6] C. Schlosser and M. Wagner, Phys. Rev. D **105**, 054503 (2022)
[7] N. Isgur and J. Paton, Phys. Rev. D **31**, 2910 (1985)
[8] T. J. Burns and F. E. Close, Phys. Rev. D **74**, 034003 (2006)
[9] M. Chanowitz and S. Sharpe, Nucl. Phys. B **222**, 211 (1985)
[10] S. Godfrey, AIP Conf. Proc. **185**, 373 (1989)
[11] T. Miyamoto and S. Yasui, Phys. Rev. D **99**, 094015 (1999)
[12] F. E. Close, Rep. Prog. Phy. **51**, 833 (1988)
[13] F. Buisseret and C. Semay, Phys. Rev. D **74**, 114018 (2006)
[14] F. Buisseret, C. Semay, V. Mathieu *et al.*, Eur. Phys. J. A **32**, 123 (2007)
[15] G. Goldhaber *et al.*, Phys. Rev. Lett. **37**, 255 (1976)
[16] I. Peruzzi *et al.*, Phys. Rev. Lett. **37**, 569 (1976)
[17] R. Brandelik, *et al.* (DASP Collaboration), Phys. Lett. B **70**,

132 (1977)
[18] R.L. Workman *et al*. (Particle Data Group), Prog. Theor. Exp. Phys. **2022**, 083C01 (2022)
[19] S. Godfrey, N. Isgur, Phys. Rev. D **32**, 189 (1985)
[20] S. Godfrey and K. Moats, Phys. Rev. D **93**, 034035 (2016)
[21] J. B. Liu and M. Z. Yang, JHEP **07**, 106 (2014)
[22] J. B. Liu and M. Z. Yang, Phys. Rev. D **91**, 094004 (2015)
[23] M. Shah, B. Patel, and P. C. Vinodkumar, Phys. Rev. D **90**, 014009 (2014)
[24] M. Shah, B. Patel, and P. C. Vinodkumar, Eur. Phys. J. C **76**, 36 (2016)
[25] J. B. Liu and C. D. Lu, Eur. Phys. J. C **77**, 312 (2017)
[26] D. Ebert, R. N. Faustov, and V. O. Galkin, Eur. Phys. J. C **66**, 197 (2010)
[27] M. Di Pierro and E. Eichten, Phys. Rev. D **64**, 114004 (2001)
[28] M. Kalinowski and M. Wagner, Phys. Rev. D **92**, 094508 (2015)
[29] G. Moir, M. Peardon, S.M. Ryan *et al*., JHEP **05**, 021 (2013)
[30] G. K. C. Cheung, C. O'Hara, G. Moir *et al*., JHEP **12**, 089 (2016)
[31] C. B. Lang, L. Leskovec, D. Mohler *et al*., Phys. Rev. D **90**, 034510 (2014)
[32] G. S. Bali, Phys. Rev. D **68**, 071501 (2003)
[33] H. Y. Cheng and W. S. Hou, Phys. Lett. B **566**, 193 (2003)
[34] K. Terasaki, Phys. Rev. D **68**, 011501 (2003)
[35] T. Barnes, F. Close, and H. Lipkin, Phys. Rev. D **68**, 054006 (2003)
[36] Y. Q. Chen and X. Q. Li, Phys. Rev. Lett. **93**, 232001 (2004)
[37] Z. Yang, G. J. Wang, J. J. Wu *et al*., Phys. Rev. Lett. **128**, 112001 (2022)
[38] R. H. Ni, J. J. Wu, and X. H. Zhong, Phys. Rev. D **109**, 116006 (2024)
[39] S. F. Chen, J. Liu, H. Q. Zhou *et al*., Eur. Phys. J. C **80**, 290 (2020)
[40] E. Eichten, K. Gottfried, T. Kinoshita *et al*., Phys. Rev. D **21**, 203 (1980)
[41] S. Godfrey, K. Moats, and E. S. Swanson, Phys. Rev. D **94**, 054025 (2016)
[42] C. Semay and B. Silvestre-Brac, Nucl. Phys. A **618**(4), 455 (1997)
[43] T. Barnes, S. Godfrey, and E. S. Swanson, Phys. Rev. D **72**, 054026 (2005)
[44] S. Kanwal, F. Akram, B. Masud *et al*., Eur. Phys. J. A **58**, 219 (2022)
[45] N. Akbar, B. Masud, and S. Noor, Eur. Phys. J. A, **47**, 124 (2011) **50**, 121(E) (2014)
[46] R. Storn and K. Price, Journal of Global Optimization **11**, 341 (1997)
[47] B. Aubert *et al*. (BaBar Collaboration), Phys. Rev. Lett. **97**, 222001 (2006)
[48] B. Aubert *et al*. (BaBar Collaboration), Phys. Rev. D **80**, 092003 (2009)
[49] R. Aaij *et al*. (LHCb Collaboration), Phys. Rev. Lett. **126**, 122002 (2021)
[50] R. Aaij *et al*. (LHCb Collaboration), Phys. Rev. D **101**, 032005 (2020)
[51] P. del Amo Sanchez *et al*. (BaBar Collaboration), Phys. Rev. D **82**, 111101 (2010)
[52] R. Aaij *et al*. (LHCb Collaboration), Phys. Rev. D **94**, 072001 (2016)
[53] R. Aaij *et al*. (LHCb Collaboration), JHEP **09**, 145 (2013)
[54] R. Aaij *et al*. (LHCb Collaboration), Phys. Rev. D. **91**, 092002 (2015) **93**, 119901(E) (2016)
[55] I. Asghar, F. Akram, B. Masud *et al*., Phys. Rev. D **100**, 096002 (2019)
[56] N. Green, W. W. Repko, and S. F. Radford, Nucl. Phys. A **958**, 71 (2017)
[57] S. F. Radford, W. W. Repko, and M. J. Saelim, Phys. Rev. D **80**, 034012 (2009)